Modeling, Optimization, and In Vitro Corneal Permeation of Chitosan-Lomefloxacin HCl Nanosuspension Intended for Ophthalmic Delivery

Ahmed Abdelbary Abdelrahman, Heba Farouk Salem, Rasha Abdelsalam Khallaf & Ahmed Mahmoud Abdelhaleem Ali

Journal of Pharmaceutical Innovation
From R&D to Market

ISSN 1872-5120

J Pharm Innov
DOI 10.1007/s12247-015-9224-7

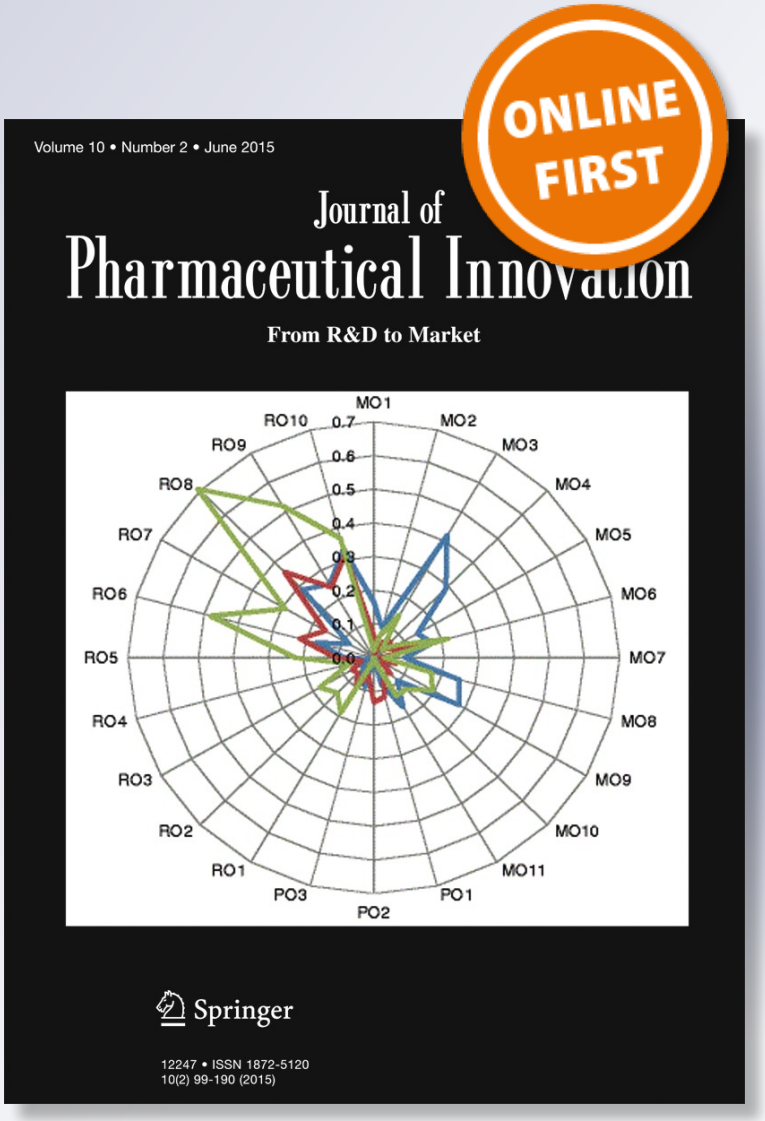

Springer

J Pharm Innov
DOI 10.1007/s12247-015-9224-7

RESEARCH ARTICLE

Modeling, Optimization, and In Vitro Corneal Permeation of Chitosan-Lomefloxacin HCl Nanosuspension Intended for Ophthalmic Delivery

Ahmed Abdelbary Abdelrahman[1] · **Heba Farouk Salem**[2] · **Rasha Abdelsalam Khallaf**[2] · **Ahmed Mahmoud Abdelhaleem Ali**[2,3]

Abstract Lomefloxacin HCl (LF) is a widely used fourth-generation fluoroquinolone antibiotic. Like most drug solutions administered via ocular route, it is usually eliminated by eye protective mechanisms. Chitosan (CS) is a natural polysaccharide polymer with numerous advantages in ocular delivery with, antibacterial, and antifungal properties. The aims were to formulate and optimize LF nanosuspensions (NS) with enhanced antimicrobial activity and prolonged duration using ionic gelation technique. Formulation variables included drug load, CS concentration, crosslinker type (tripolyphosphate and sodium alginate), and concentration. Nanosuspension properties (particle size, zeta potential, polydispersity index, entrapment efficiency, drug release, and permeation through bovine cornea) were evaluated. The artificial neural networks (ANNs) model showed optimum entrapment efficiency of 70.63 % *w/w*, particle size of 176±0.28 nm, and zeta potential of 13.65 mV. Transmission electron microscopy illustrated the production of well-defined spherical nanoparticles. The nanosuspensions showed prolonged release of LF for more than 8 h and threefold increase in amount permeated through bovine cornea compared to drug solution. Improved antibacterial activity of the nanosuspension was noted where 2- and 3.5-fold decrease in minimum inhibitory concentration (MIC) of drug against Gram-positive and Gram-negative bacteria were observed, respectively. Twofold decrease in minimum bactericidal concentration (MBC) of drug nanosuspension against both types of bacteria was also demonstrated. Histopathological examination showed compatibility of optimized formulation with eye tissues in rabbit model. Therefore, model-optimized LF nanosuspension could be an ideal solution to ocular infections by virtue of their augmented activity, high compatibility, and improved permeability.

Keywords Antibacterial activity · Chitosan · Ionic gelation · Lomefloxacin HCl · Nanosuspension optimization · Transcorneal permeation

✉ Ahmed Mahmoud Abdelhaleem Ali
ahmed.mahmoud3@yahoo.com;
ahmed.abdelhalem@pharm.bsu.edu.eg

Ahmed Abdelbary Abdelrahman
ahmedmahmoud3@gmail.com

Heba Farouk Salem
heba_saleem2004@yahoo.co.uk

Rasha Abdelsalam Khallaf
Rasha_khallaf@yahoo.com

[1] Department of Pharmaceutics, Faculty of Pharmacy, Cairo University, Cairo, Egypt

[2] Department of Pharmaceutics and Industrial Pharmacy, Faculty of Pharmacy, Beni-Suef Univeristy, Shehata Hegazi Street, P.O. Box 62514, Beni Suef, Egypt

[3] Department of Pharmaceutics, Faculty of Pharmacy, Taif Univeristy, Taif, Saudi Arabia

Introduction

Lomefloxacin hydrochloride (LF) is a widely used antibacterial in the treatment of both Gram-negative and Gram-positive bacterial infections [1]. Based on physicochemical properties of fluoroquinolones and in vitro permeation [2], recent studies on biopharmaceutics classification system (BCS), confirmed that lomefloxacin HCl may belong to class I being highly soluble and permeable [3]. However, changes in the physiological pH either at the site of administration or site of absorption may increase the tendency of the drug to develop positive or negative surface charges rather than formation of the neutral or zwitterionic forms [4]. These changes, either due to the drug formulation or the physiological environment, will

Published online: 07 June 2015

inevitably lead to unpredictable bioavailability and/or antimicrobial activity of the drug through changes in the liberation of drug from dosage forms and/or its penetration at absorption or activity sites [5]. Therefore, temporary change of the substrate in the form of nanoparticles could be a helpful strategy to overcome the aforementioned challenges. Many routes of administration, including oral, parental, and ophthalmic, were used for delivery of LF. However, delivery through the ocular route is limited due to high tear fluid turnover, nasolachrymal drainage, and metabolic enzymes present in tear fluid [6]. Other obstacles facing treatment of ocular infections include patient incompliance, difficulty to maintain the required dose at site of action, and the limited transcorneal permeation of applied drugs [7]. Therefore, nanosuspensions could be a more suitable drug delivery system for the ocular route of administration [8]. Ocular nanosized drug delivery systems protect the ocular-instilled drugs from metabolism by tear fluid enzymes and increase their permeation through corneal membranes [9–11]. Ocular drug delivery systems in the form of nanosuspensions also have the added advantage of being able to prolong drug release at the site of action [12]. Several nanosuspension formulations have been developed and successfully used for topical ocular drug delivery [13–16]. Polymeric nanoparticles have been widely investigated as a possible tool for carrying ocular drugs [17]. Chitosan (CS) is a biodegradable polysaccharide polymer that has mucoadhesive characters that help increase the contact to ocular tissues and hence provide prolonged drug delivery. In addition, CS can increase corneal permeation of ocular drug by acting as a penetration enhancer [18]. Moreover, CS is well tolerated by ocular tissues and showing no irritation signs such as redness or edema following ocular administration [19]. Chitosan was also reported to have both antibacterial and antifungal properties [20, 21] making the polymer a good candidate for sterile dosage forms such as ophthalmic formulations. In order to form nanoparticles, CS is usually crosslinked using a polyanion or another negatively charged polymer. Such formulations often require careful adjustment of types and levels of components to produce stable nanosuspensions. Modeling and optimization of nanosuspensions using artificial neural networks (ANNs) have been frequently used in the literature to obtain the optimum desired properties [22–24].

The aims of work in this study addressed formulation and evaluation of LF nanosuspension using CS as a carrier in order to enhance its antibacterial activity, improve its corneal permeation, and prolong its ocular activity leading to maximized bioavailability. The work focused on modeling of nanoparticle characteristics and permeability. This linkage between nanoparticle attributes and effects (permeability and antibacterial activity) was not done before for lomefloxacin HCL in eye tissues. Modeling and optimization of LF-CS nanosuspensions was followed by experimental evaluation of the antibacterial properties of the model proposed formulation using minimum inhibitory concentration (MIC) and the minimum bactericidal concentration (MBC) compared to drug solution.

Materials and Methods

Materials

Lomefloxacin HCl was obtained as a gift sample from October Pharma, Egypt. Chitosan was purchased from Sigma Aldrich, UK, through the Egyptian Import Center, Naser City, Cairo, Egypt. Tripolyphosphate (TPP) and sodium alginate (Na ALG) were purchased from Prolabo, France. Other chemicals were of analytical grade and obtained from the El Nasr chemical company, Cairo, Egypt.

Preparation of LF-CS Nanosuspensions

Preparation of LF-CS nanosuspension was carried out according to the method reported by Motwani et al. [25] with modification. First, different concentrations of CS (0.1, 0.2, and 0.3 % *w*/*v*), TPP, and Na ALG (0.2, 0.4, and 0.6 % *w*/*v* of each) solutions were separately prepared through dissolving the required amounts in acetate buffer (pH 5) until no residues were observed (Table 1). Chitosan solutions were prepared by dissolving the required amounts also in acetate buffer (pH 5) then the pH was slightly raised to 5.7 using 1 N NaOH while the pH of crosslinker solutions was kept at a lower value (pH 5.3) to ensure complete ionic interaction. Then, the required amounts of LF (10 or 15 mg) were dissolved in 10 mL of the previously prepared chitosan solution until no residues were observed. Crosslinking was achieved by slowly dropping 5 mL of TPP or Na alginate solution to the CS solution under homogenization at 8000 rpm using high shear homogenizer (yellow line DI 25 basic, Germany) for 20 min. The formed nanoparticles were collected by centrifugation at 20,000 rpm using a cooling centrifuge (Sigma, 3-30K, Germany) for 30 min at 4 °C and kept in a refrigerator for further studies.

Determination of the Entrapment Efficiency

Free LF (un-entrapped) was separated from entrapped LF by centrifugation [26] of the nanosuspension using cooling centrifuge (Sigma, 3-30K, Germany) at 20,000 rpm for 30 min. The collected nanoparticles was then washed with distilled water and re-centrifuged to ensure complete removal of the un-entrapped drug. The amount of un-entrapped LF was determined after dilution of 0.1 mL of the supernatant to 10 mL using acetate buffer pH 5. Three replicates of this solution were analyzed spectrophotometrically at 282 nm using Jasco

Table 1 Composition of lomefloxacin loaded chitosan nanosuspensions

Formula no.	Lomefloxacin HCl (mg)	Crosslinker type	Chitosan concentration (% *w/v*)	Crosslinker concentration (% *w/v*)
C1	10	TPP	0.1	0.2
C2	10	TPP	0.1	0.4
C3	10	TPP	0.1	0.6
C4	10	TPP	0.2	0.2
C5	10	TPP	0.2	0.4
C6	10	TPP	0.2	0.6
C7	10	TPP	0.3	0.2
C8	10	TPP	0.3	0.4
C9	10	TPP	0.3	0.6
C10	10	Na ALG	0.1	0.2
C11	10	Na ALG	0.1	0.4
C12	10	Na ALG	0.1	0.6
C13	10	Na ALG	0.2	0.2
C14	10	Na ALG	0.2	0.4
C15	10	Na ALG	0.2	0.6
C16	10	Na ALG	0.3	0.2
C17	10	Na ALG	0.3	0.4
C18	10	Na ALG	0.3	0.6
C19	15	TPP	0.2	0.4
C20	15	TPP	0.2	0.6
C21	15	Na ALG	0.2	0.4
C22	15	Na ALG	0.2	0.6

TPP tripolyphosphate, *Na ALG* sodium alginate

spectrophotometer (Jasco V-530, Japan). The percentage of entrapped LF was determined [27] using Eq. 1.

$$\%\text{Entrapped LF} = \frac{\text{Total LF} - \text{Free LF}}{\text{Total LF}} \times 100 \quad (1)$$

Determination of Particle Size and Zeta Potential

In order to detect the stability of the produced LF nanosuspension, particle size (PS), zeta potential (ZP), and polydispersity index (PDI) properties were measured by diluting 1.0 mL of CS nanosuspension to 5 mL by distilled water. The diluted nanosuspension was measured using Zetasizer Nano (Malvern Instruments, UK).

Transmission Electron Microscopy

In order to determine the morphology of the produced nanoparticles, one drop of the nanosuspension was applied on a copper grid and left to dry. Then, one drop of phosphotungestic acid (positive stain) was added to the dry nanoparticles. Finally, the nanoparticles were examined using transmission electron microscope analyzer operated at an accelerating voltage of 80 kV (Jeol, Japan).

In Vitro Release Study

Drug release from LF-CS nanosuspension was carried out according to a reported method with modification [28]. Different volumes of nanosuspension formulations containing the same calculated amount of LF (4 mg) were transferred to a cylindrical glass tube (7.5 cm in length and 2.5 cm in diameter). The open end of the tube was sealed with a dialysis membrane (MW cut off 12,000 kDa). The tube was inverted and suspended in 500-mL simulated tear fluid (STF) composed of sodium bicarbonate 0.2 %, calcium chloride 0.008 %, and sodium chloride 0.67 % adjusted to pH 7.4. The tube was assembled vertically inside the dissolution flask of USP dissolution apparatus II (Hanson Research, SR8 plus model, Chatsworth, USA) so that the membrane touches the surface of the medium. The temperature was kept at 37± 0.5 °C and the glass tubes (attached to the vertical basket holder) were allowed to rotate at a velocity of 50 rpm. At predetermined time intervals, 5 mL of the medium was withdrawn for UV analysis and the volume of receptor compartment was maintained with an equal volume of fresh STF.

In Vitro Transcorneal Permeation, Corneal Hydration, and Irritation Studies

Transcorneal permeation was carried out using modified Franz diffusion cell [29]. The freshly dissected bovine corneal membranes were inserted between the donor and the receptor chamber of the diffusion cell where the corneal surface faces the donor compartment. The receptor compartment was filled with 50 mL pH 7.4 Krebs ringer solution (KRS) [30] while the donor compartment contained different volumes of LF nanosuspension carrying fixed weights of LF. The receptor chamber was stirred at 50 rpm on a magnetic stirrer at 37± 0.5 °C. One milliliter was withdrawn from receptor chamber (at predetermined time intervals for 24 h), filtered via 0.45-μm Millipore filter then diluted to 3 mL (with KRS) and finally measured spectrophotometrically at 282 nm. Experiments were done in triplicates and the average values were calculated. The permeation parameters including the cumulative amount of the drug permeated per unit area after 24 h (Q_{24} in μg/cm^2), the time required to start permeation (lag time in min) and the permeability coefficient (Kp) were calculated. The values of Kp for each formula was obtained by dividing the slope of the straight line portion of the permeation curve by the concentration of drug originally added. Comparisons were made against drug solution [31]. The corneal hydration test was carried out to detect the safety of the prepared formulations. In this test, after removal of the scleral ring; each corneal sample was then desiccated at 100 °C for 6 h to give the corresponding dry corneal weight (Wd). Then, the cornea was subjected to the permeation test mentioned earlier, after which it was reweighed to get the hydrated weight (Wt). The percent corneal hydration (% CH) [32] was measured using Eq. 2.

$$\%CH = (1-(Wd/Wt)) \times 100 \quad (2)$$

The ocular irritation study was carried out to test for compatibility of the prepared nanosuspension formulation with eye tissues in the rabbit model [33]. Six New Zealand rabbits were divided into two groups, each composed of three rabbits. The first group received the optimized LF-loaded CS nanosuspension in the right eye. The second group received drug-free CS nanosuspension. The left eye was not treated and served as control in both groups. Treatments were continued twice daily for a period of 1 week. The signs of irritation in rabbits eyes (redness, swelling, or excessive tearing) were detected using slit lamp (Optolab Zone, India) at time intervals of 1, 24, 48, 72 h, and 1 week. At the end of the treatment period, the animals were anesthetized and sacrificed. Eyes and eyelids were removed and kept in Davidson fixative solution for 24 h. Then, the organs were dehydrated and stabilized with formalin solution and stored in low-melting paraffin. Finally, cut sections were stained with hematoxylin and eosin for histological examination [34]. This experiment was conducted after obtaining a formal ethical approval from the animal ethical committee at Beni-Suef University.

Modeling and Optimization of Nanosuspension Formulation

Nanosuspension formulation data set was composed of 22 records based on different input variables. These included drug load, crosslinker type, chitosan concentration, and crosslinker concentration. The crosslinker types were coded with numerical values as follows: TPP (1) and Na ALG (2). The measured dependent variables included percentage entrapment efficiency (%EE) average nanoparticle size (PS), average zeta potential (ZP), and average polydispersity index (PDI), percentage drug released after 8 h (%Rel-8 h), time prior to start of drug permeation (lag time), cumulative amount of drug permeated through corneal tissue within 24 h (Q_{24}) and permeation coefficient (Kp). Modeling and optimization of the data was carried out using artificial neural networks (ANNs)—genetic algorithm software package (INForm V3.6, Intelligensys Ltd., UK). This modeling tool is based on a multi-layer perceptron (MLP) network embedded into the program which is responsible for model training using the entered data to build up the cause-effect relationships [35]. The experimentally collected data set was divided into training records (80 %), testing records (10 %), and validation records (10 %) for model training, testing the predictability, and model validation, respectively. Predictability of trained models was evaluated by the correlation coefficient *R*-square (R^2) values computed automatically during training, testing, and validation steps (Eq. 3). High R^2 values closer to unity indicate appropriate predictability of the trained model [36]. The following formula was derived from ANOVA statistics generated by the modeling software:

$$R^2 = 1-\frac{\sum_{i-1}^{n}\left(y_i-y_i^*\right)^2}{\sum_{i-1}^{n}\left(y_i-y_i^-\right)^2} \times 100 \quad (3)$$

Where y_i is the individual value of the dependent variable, y_i* is the predicted value from the model and y_i^-; is the mean of the dependent variable. In this formula, the numerator represents the sum of squares for the error term (SSE) and the denominator represents the total sum of variable is accounted for in the model. The artificial neural network structure I(4)-H(2)-O(1) was used for model training (linking inputs and the output properties), with four nodes representing the input layer, two nodes in the hidden layer, and one node in the output layer. Trusted models should result in validation correlation R^2 as high as those obtained during model training and testing. The root mean squared errors (RMSE) were also calculated and compared to those of training and testing.

After developing of the predictive models for each property, optimization was carried out by setting the desired constraints on some process variables (e.g. setting integer numbers to the crosslinker type). The desired range for each of the output properties was entered into the model optimization step and the desirability function was selected as "tent" in the model optimization window [37]. The specified minimum and maximum values for the output properties were assigned as follows; %EE (68–75 %), PS (150–300 nm), ZP (9.5–15), PDI (0.1–0.3), %Rel-8 h (78–90 %), Q_{24} (500–700 μg), lag time (10–20 min), and Kp (0.3–0.6). The model-generated solution demonstrates a suggested optimized formula for the nanosuspension which was then prepared and characterized and the results compared to the predicted counterparts.

Microbiological Studies

The antibacterial activity of the optimized formula and LF solution were tested using the clinical laboratory standard institute (CLSI) broth microdilution technique [38]. The medium used in the study was composed of Muller-Hinton Broth (Oxoid) placed in a 96-well cell microtiter plate (Corning Incorporated, Corning, USA). Serial dilutions of LF solution and optimized nanosuspension starting from 500 to 4.76×10^{-4} μg/mL were prepared and placed in 20 wells. A number equivalent to 1×10^{6} colony forming units per milliliter (cfu/mL) of tested microorganism (*Escherichia coli* ATCC 5087 and *Bacillus subtilis* ATCC 6633) were inoculated in these wells by overnight culture. In well number 20, the bacteria were allowed to grow freely (turbidity control). After incubating the inoculated wells for 24 h at 37 °C, microbial growth was determined through measuring turbidity at 620 nm by a microtiter plate reader (Labsystem iEMS reader, Helsinki, Finland) [39]. The MIC was considered as the average of the last clear tube and first turbid tube. The MBC was calculated after culturing last three clear tubes on Muller-Hinton agar medium and examining the absence of growth.

Results and Discussion

Entrapment Efficiency

The percentage entrapment of LF into CS nanoparticles was found to vary between 57.23 and 80.03 % *w/w* (Table 2). The highest level was obtained when CS, TPP, and Na ALG were at medium concentration. It was also noticed that Na ALG gave higher entrapment efficiency compared to TPP polymer. This might be due to the fact that Na ALG is a bulky molecule so it can decrease the ability of the drug to diffuse out of nanoparticles. Increasing drug concentration led to increasing entrapment efficiency, which correlates well with other studies performed on rifampicin entrapped into CS nanoparticles [40].

Particle Size, Zeta Potential, and Polydispersity Index

Particle size of prepared nanosuspensions ranged from 57 to 520 nm (Table 2). The results indicated that increasing polymer concentrations led to an increase in particle size, as reported for similar nanosuspension particle size increased with polymer concentration. Polydispersity indices (PDI) of CS nanoparticles ranged from 0.016 to 0.57. The increase in PDI of CS nanoparticles was found to be dependent on polymers concentration as increasing polymers concentration led to increase in PDI. Increasing amount of drug used resulted in increasing the particle size and polydispersity index of CS nanoparticles. The wide range of zeta potential values (8.33—40 mV) could be explained on the basis of polymer concentrations and structure. It was well observed that zeta potential values increased linearly with increasing CS concentration. This phenomena can be explained by the presence of highly protonated amine groups at higher CS concentrations, similar results were reported By Gan and Wang [41]. On the other hand increasing TPP and Na ALG resulted in a decrease in zeta potential values; this could be understood in the light of the electrostatic interaction between the negatively charged moieties present in TPP and Na ALG and the positively charged amine group present in CS which resulted in a decrease in the positive charges present on nanoparticles' surface as reported by Boonsongrit et. al [42]. The use of the crosslinker Na ALG yielded much lower zeta potential values compared to TPP crosslinker. This can be a result of the greater shielding effect that eventually led to decreasing the overall available positive charges. The increase in LF amount increased zeta potential values this might be due to the increasing number of positive charges as a result of hydrogen ions obtained by drug solubilization.

Morphology of the Prepared Nanoparticles

Transmission electron microscopy (TEM) of LF-loaded nanoparticles (Fig. 1) illustrated that LF-loaded CS nanoparticles were spherical, smooth, and dense which show the ability of the used polymers to interact and form typical nanoparticles. However, differences in nanoparticles' morphology were noted due to different chitosan and crosslinker concentrations. Figure 1 illustrates TEM of formula C1 (composed of the lowest concentrations of both CS and TPP), where smaller nanoparticles can be observed (Fig. 1a). The TEM of formula C10 (composed of the lowest concentrations of both CS and Na ALG) showed larger and more rounded particles (Fig. 1b).

In Vitro Release Studies

The in vitro release data revealed the slow release of LF from nanosuspension formulations for more than 8 h. The highest release percentage was obtained from formula C1 which

Table 2 Lomefloxacin-chitosan nanosuspension formulation variables and measured properties

Formula no.	Crosslinker type	Chitosan (% *w/v*)	Crosslinker (% *w/v*)	Drug (mg)	% Entrapment efficiency	Zeta potential (mV)	Particle size (nm)	PDI	%. Drug released 8 h	Q_{24} (μg/cm^2)	Lag time (min)	Permeation coefficient (Kp)
1	1.00	0.10	0.20	10.00	57.23	27.90	57.03	0.02	93.60	719.60	6.00	0.74
2	1.00	0.10	0.40	10.00	63.24	24.90	79.85	0.21	91.40	693.03	7.00	0.61
3	1.00	0.10	0.60	10.00	58.67	22.80	124.50	0.22	88.77	633.18	8.20	0.38
4	1.00	0.20	0.20	10.00	67.39	32.00	77.77	0.24	90.09	687.00	8.00	0.51
5	1.00	0.20	0.40	10.00	75.09	28.00	101.00	0.24	86.85	652.18	10.00	0.42
6	1.00	0.20	0.60	10.00	69.38	26.50	157.70	0.29	83.22	620.26	11.00	0.37
7	1.00	0.30	0.20	10.00	63.24	40.00	105.50	0.31	87.02	624.60	8.50	0.49
8	1.00	0.30	0.40	10.00	69.26	34.00	150.70	0.33	84.99	560.84	12.00	0.44
9	1.00	0.30	0.60	10.00	69.02	28.00	222.60	0.38	81.01	522.38	15.00	0.31
10	2.00	0.10	0.20	10.00	60.54	11.80	113.90	0.27	85.40	603.35	9.50	0.48
11	2.00	0.10	0.40	10.00	67.03	10.10	192.10	0.29	81.11	548.05	11.50	0.40
12	2.00	0.10	0.60	10.00	64.63	8.33	244.50	0.33	77.59	483.45	14.00	0.30
13	2.00	0.20	0.20	10.00	74.61	15.70	125.30	0.36	78.30	595.32	12.00	0.44
14	2.00	0.20	0.40	10.00	78.28	12.00	203.20	0.41	74.30	543.39	16.00	0.36
15	2.00	0.20	0.60	10.00	75.69	9.34	348.60	0.49	69.89	462.06	19.00	0.29
16	2.00	0.30	0.20	10.00	62.52	20.70	151.30	0.49	75.44	573.67	14.00	0.34
17	2.00	0.30	0.40	10.00	69.14	16.30	389.60	0.51	68.35	427.40	20.00	0.26
18	2.00	0.30	0.60	10.00	67.95	13.60	520.50	0.56	63.43	317.25	29.00	0.20
19	1.00	0.20	0.40	15.00	79.42	31.00	143.60	0.27	83.22	628.60	10.50	0.40
20	1.00	0.20	0.60	15.00	76.48	29.60	205.50	0.31	80.59	593.44	14.00	0.29
21	2.00	0.20	0.40	15.00	80.03	19.60	390.40	0.51	73.61	523.19	18.00	0.32
22	2.00	0.20	0.60	15.00	77.08	16.00	409.90	0.57	69.15	441.10	21.00	0.29

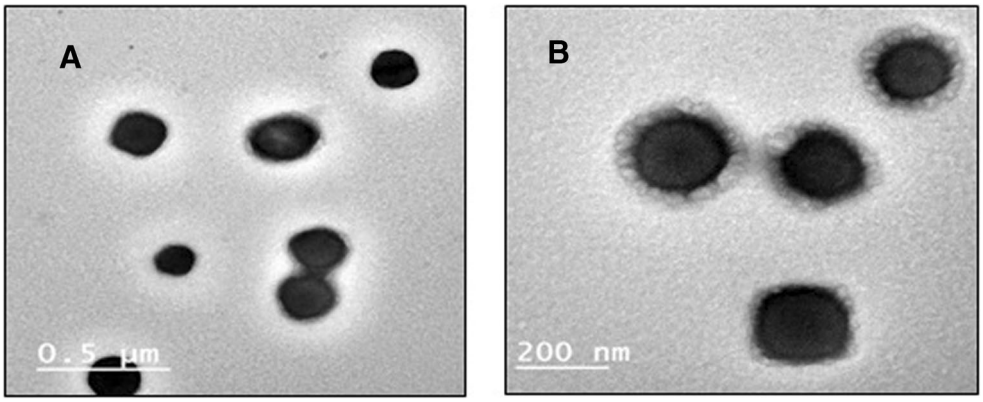

Fig. 1 Transmission electron micrographs of lomefloxacin-chitosan nanoparticles using tripolyphosphate (**a**) and sodium alginate (**b**) as crosslinker

released more than 93.63 % after a period of 8 h while LF powder released 90 % after 30 min. It was also noted that the nanosuspensions exhibited a biphasic release pattern where 18–57 % of LF were released during the first hour, then the release was extended to 8 h. This could be attributed to the fast release of drug molecule more adjacent to the surface of nanoparticles followed by a slow release due to drug diffusion from inside the polymeric matrix. This biphasic release behavior was observed by other researchers working on chitosan nanosuspensions as reported in the literature [43–46]. It was also observed that formulations containing TPP as the crosslinker showed higher release percentages compared to

Table 3 ANOVA statistics obtained by the model for LF nanosuspension properties (% EE, average PS, Average PDI, and average ZP)

Property	Source of variation	Sum of squares	Degrees of freedom	RMSE	Mean sum of squares	Computed *F* ratio
% EE	Model	605.814	13	6.83	46.6011	1.64837
	Error	56.5422	2	5.32	28.2711	
	Total	677.17	15			
	Covariance term	Sum of errors				
	14.814	−6.19551				
	Train set *R*-squared	91.65 %				
	Test set *R*-squared	88.56 %				
Average PS (nm)	Model	211627	13	127.59	16279	2.57033
	Error	12,666.9	2	79.58	6333.44	
	Total	243,932	15			
	Covariance term	Sum of errors				
	19,637.6	−108.162				
	Train set *R*-squared	94.81 %				
	Test set *R*-squared	79.70 %				
Average PDI	Model	0.275403	13	0.15	0.0211848	5.71236
	Error	0.00741719	2	0.06	0.00370859	
	Total	0.2877	15			
	Covariance term	Sum of errors				
	0.00488024	0.0771123				
	Train set *R*-squared	97.42 %				
	Test set *R*-squared	98.18 %				
Average ZP (mV)	Model	1262.21	13	9.85	97.0934	32.6498
	Error	5.94757	2	1.72	2.97378	
	Total	1249.99	15			
	Covariance term	Sum of errors				
	−18.1719	1.16756				
	Train set *R*-squared	99.52 %				
	Test set *R*-squared	98.68 %				

Table 4 ANOVA statistics obtained by the model for nanosuspension properties (% LF released in 8 h, lag time, cumulative LF permeated in 24 h (Q_{24}) and permeation coefficient Kp)

Property	Source of variation	Sum of squares	Degrees of freedom	RMSE	Mean sum of squares	Computed *F* ratio
% LF released in 8 h	Model	1103.67	13	9.20	84.8976	13.0015
	Error	13.0596	2	2.60	6.52981	
	Total	1150.51	15			
	Covariance term	Sum of errors				
	33.7836	−1.03077				
	Train set *R*-squared	98.86 %				
	Test set *R*-squared	97.80 %				
Q_{24} h	Model	142080	13	104.5	10929.2	2.61083
	Error	8372.23	2	64.70	4186.11	
	Total	164,840	15			
	Covariance term	Sum of errors				
	14,387.3	−31.0813				
	Train set *R*-squared	94.92 %				
	Test set *R*-squared	87.07 %				
Lag time (min)	Model	484.26	13	6.10	37.2508	3.46445
	Error	21.5046	2	3.28	10.7523	
	Total	533.55	15			
	Covariance term	Sum of errors				
	27.785	1.70422				
	Train set *R*-squared	95.97 %				
	Test set *R*-squared	98.06 %				
Permeation coefficient (Kp)	Model	0.265944	13	0.14	0.0204572	5.31525
	Error	0.00769756	2	0.06	0.00384878	
	Total	0.272175	15			
	Covariance term	Sum of errors				
	−0.00146645	−0.12436				
	Train set *R*-squared	97.17 %				
	Test set *R*-squared	94.76 %				

those containing Na ALG. This could be due to the smaller particle size exhibited by formulations containing TPP compared to those containing Na ALG and the shorter path length during drug diffusion. The in vitro release data were analyzed according to zero-order, first-order, and Higuchi release kinetics. The highest regression R^2 values (>0.999) were shown for LF released from the nanosuspensions according to the Higuchi diffusion model, while LF released from LF powder followed first-order kinetics. these results are supported by other reports that confirm drug release from CS nanoparticles with the diffusion-controlled mechanism [47].

In Vitro Transcorneal Permeation

Permeation parameters (Lag time, $Q_{24,}$ and Kp) calculated for each nanosuspension formulation compared to LF solution are shown in Table 2. It was observed that CS increased the permeation of LF from all nanosuspension formulations compared to LF solution. This increase can be explained in the light of CS interesting biological properties. It was reported that CS as a penetration enhancer can help in the opening of the very small junctions present between ocular epithelial cells [48]. Another suggested mechanism for better corneal permeation of CS nanoparticles is the presence of intracellular pathways through which CS nanoparticles can effectively deliver the required dose [49]. The obtained results revealed that permeation parameters decreased with increasing concentration of polymers, which could be explained by increase in particle size and decreases in the surface area available for permeation. It was noticed that nanosuspensions containing TPP have better permeation parameters compared to those containing Na ALG, this might also be due to the smaller particle size produced in case of nanoparticles containing TPP compared to those containing Na ALG. Consequently, TPP containing nanoparticles can offer a greater surface area for LF permeation through cornea. It was also observed that the increased amount of LF resulted in a decrease in the permeation parameters. This result may support the active transport mechanism

by which the free drug is absorbed or the efflux behavior as previously reported in the literature [2]. Significant differences in lag time, Q_{24} hours, and Kp between nanosuspensions and free drug solutions were demonstrated ($P<0.001$).

Nanosuspension Modeling and Optimization

Modeling of nanosuspension formulation showed a high predictive quality model as demonstrated by high training and testing R^2 values (>90 %) as shown in Tables 3 and 4. The calculated RMSE values were also small and comparable between model training and testing (6.83 and 5.32 for %EE, 9.20 and 2.60 for %Released, and 6.10 and 3.28 for lag time) which indicate model trust ability (Tables 3 and 4). Model validation resulted in high R^2 values (82–96 %) indicating model validity for prediction and optimization. The model optimized formulation for LF nanosuspension was composed of 11 % LF, 0.1 % chitosan, and 0.5 % Na ALG as the crosslinker (Table 5). The desirability of the obtained model approached 0.99 which represents high closeness of the obtained model predictions from the desired values entered during optimization. The experimental evaluation of the optimized formulation indicated similar properties where, the actual %EE was 66.50 % and particle size was found to be 149 nm relative to the model-predicted value of 70.60 and 176 nm, respectively. Also, other insignificant differences between the actual and model-predicted properties including ZP, PDI, %Rel-8 h, Q_{24}, Lag time, and Kp were also demonstrated (Table 5).

Response Surface Plots

The relationship between nanosuspension formulation variables and output properties were summarized by the response surface plots obtained from the modeling step (Figs. 2, 3, 4, and 5). The entrapment efficiency was increased by increasing the concentration of Na ALG crosslinker above the value of 0.35 % *w/v* (Fig. 2a). The increase in concentration of both CS and LF were found to increase the %EE (Fig. 2b), which was expected due to greater tendency for entrapment. The average nanoparticle size was found to increase by increasing the concentration of Na ALG above 0.35 % *w/v* (Fig. 2c). This finding may suggest that the 0.35 % concentration of Na ALG can be considered as a lower and upper threshold values for optimum entrapment efficiency and nanoparticles size, respectively. In the same way, the average PS was increased by increasing the drug concentration and chitosan concentration above 0.2 % *w/v* (Fig. 2d). The effect of the crosslinker type on the ZP indicated that massive decrease in ZP was obtained with Na ALG compared to that of TPP as indicated by the high blue tip of the response surface referring to high ZP and the flat base of the 3D plot at crosslinker type 2 (Na ALG), referring to the lowest ZP (Fig. 3a). This observation could be attributed to the stronger steric stabilization and neutralization effects of

Table 5 Model optimized solution and the experimental application of the suggested nanosuspension formulation

Solution	Desirability	X1 Crosslinker type	X2 Chitosan conc. (% *w/v*)	X3 Crosslinker conc. (% *w/v*)	X4 Drug conc. (mg)	Y1 EE (%)	Y2 Zeta	Y3 Size	Y4 PDI	Y5 % Released (8 h)	Y6 Q_{24}	Y7 Lag time	Y8 Permeation coeff. (Kp)
Model predicted	1	2	0.11	0.50	10.95	70.63	13.65	176.36	0.28	81.86	574.86	10.61	0.38
Experimental	1	2	0.11	0.50	10.95	66.50	10.91	149.12	0.26	84.03	591.61	9.50	0.37

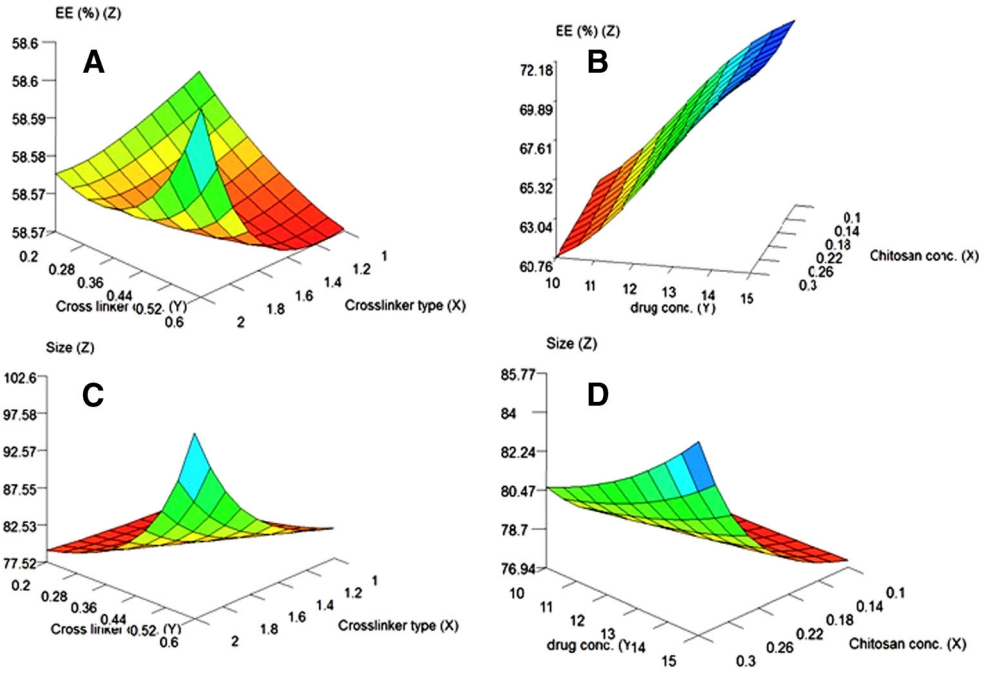

Fig. 2 Response surface plots showing effects of nanosuspension formulation independent variables on % entrapment efficiency (**a**, **b**) and nanoparticle size (**c**, **d**)

the alginate molecules on the surface of nanoparticles. The increase in concentration of the drug and chitosan were found to increase ZP, which is expected by such charged molecules (Fig. 3b). The polydispersity index increased with increase in crosslinker type and concentration and the effect of alginate was higher than that of TPP (Fig. 3c). The effect of chitosan concentration on increasing the PDI was found to be higher than that of drug concentration (Fig. 3d). The high variability in PDI is almost due to the fact that the nanosuspension is a multi-component system containing different polymers and drug particles. In Fig. 4a, the increased concentration of Na ALG led to a strong decrease in percentage LF released in 8 h while high release percentage was obtained with TPP (Fig. 4a). Also, increasing the chitosan concentration was found to produce a larger decrease in the percentage of LF released (Fig. 4b). The cumulative amount of LF permeated through corneal tissues in 24 h (Q_{24}) reached the maximum at low concentrations of the crosslinker TPP and the minimum values were obtained at high concentrations of alginate (Fig. 4c) due to larger size of the alginate molecule. The lag

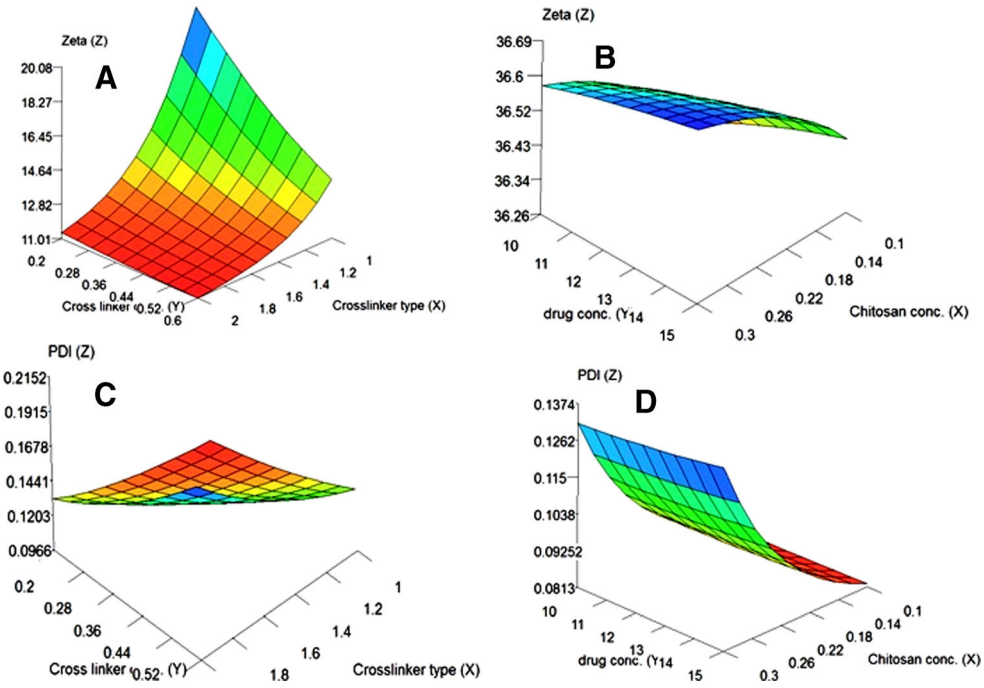

Fig. 3 Response surface plots showing effects of nanosuspension formulation independent variables on zeta potential (**a**, **b**) and polydispersity index (**c**, **d**)

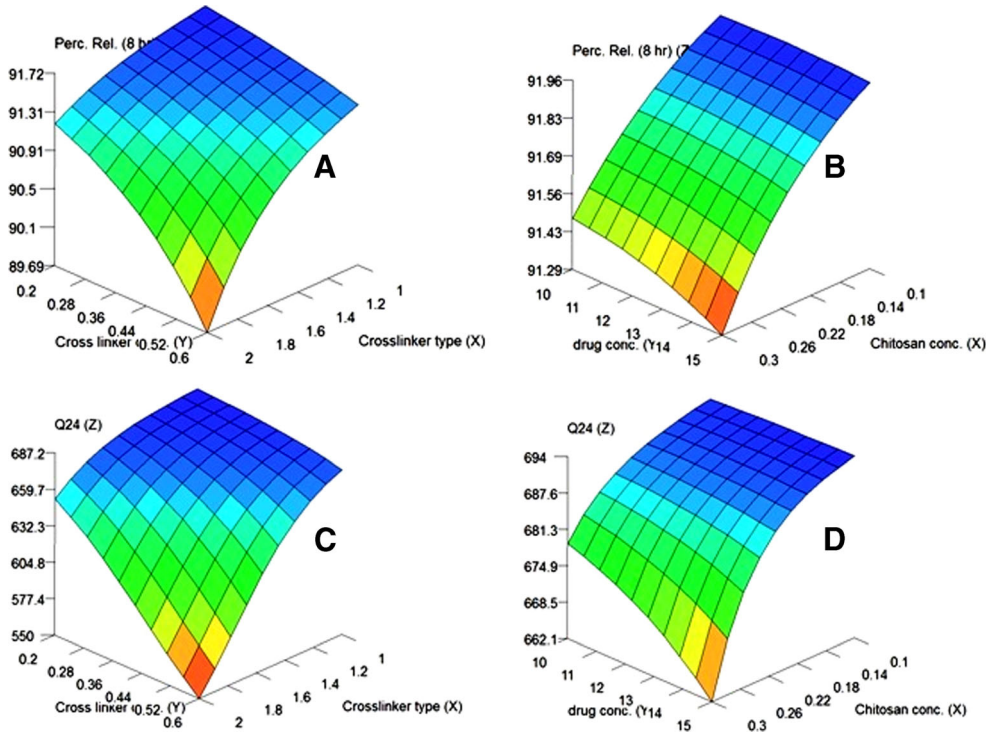

Fig. 4 Response surface plots showing effects of nanosuspension formulation independent variables on percentage drug released in 8 h (**a**, **b**) and in vitro cumulative drug permeated through corneal tissues in 24 h (**c**, **d**)

time prior to drug permeation was found to increase by increasing the concentration of the alginate crosslinker while the minimum lag time was observed at low concentrations of TPP (Fig. 5a). The highest permeation coefficient (Kp) of LF was achieved at the lowest concentration of the TPP crosslinker while the alginate polymer showed low Kp values (Fig. 5c). Increasing concentration of both LF and CS showed decreased permeation coefficient values which might be due to increased particle size and viscosity of the medium during crosslinking at such higher concentrations (Fig. 5d). The above results indicated that the minimum values of Q_{24}, Kp, and lag time could be achieved at low concentration of chitosan using low to medium concentration of TPP crosslinker rather than Na ALG. While the optimum values of all attributes could be reached, if NA ALG was used as the crosslinker and low concentrations of both the drug and chitosan as shown by

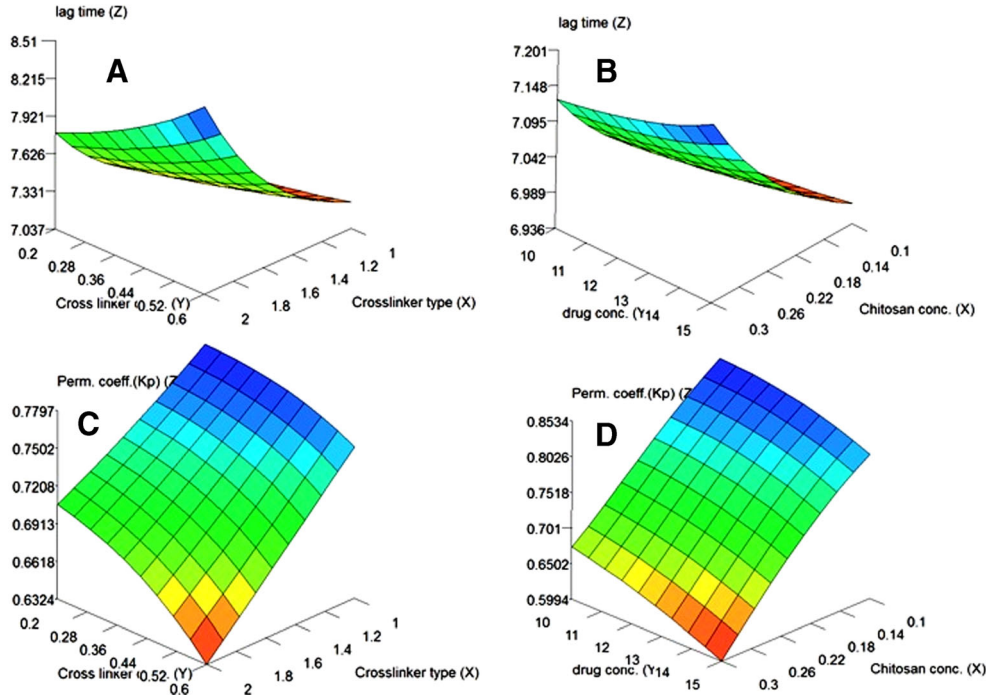

Fig. 5 Response surface plots showing effects of nanosuspension formulation independent variables on lag time prior to drug permeation (**a**, **b**) and permeation coefficient, Kp (**c**, **d**)

the optimization results in Table 5. The modeling using ANNs has shed the light on certain threshold values such as the threshold concentrations of Na ALG 0.35 % *w/v* and chitosan 0.2 % *w/v* which demonstrated variable nanoparticle size, release, and permeability properties below and above this limit. Also, the large differences in ZP, %LF released, and permeability coefficient due to different crosslinker type and concentration were better explained and understood visually by the shape of the response surface plots illustrating the importance of ANNs in the modeling and optimization of the nanosuspension (Figs. 3–5).

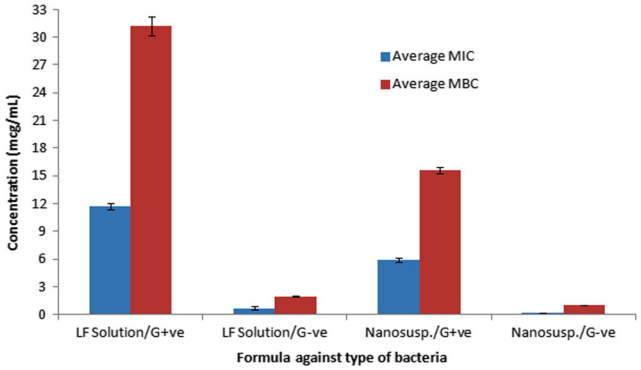

Fig. 7 Microbiological activity of LF-loaded CS nanoparticles and free LF solution against Gram +ve (*Bacillus subtilis*) and Gram –ve (*E. coli*) bacteria

Corneal Hydration and Irritation Studies

The safety of ocular formulations on the corneal tissues was measured by evaluation of the corneal hydration and irritation. The normal hydration of cornea falls in the range of 76–80 % of its dry weight and higher hydration levels (83–92 %) indicate damage of corneal tissues [50]. In this study, corneal hydration remained in the normal range of 76–79.90 %. Thus, the produced formulation could be considered safe and non-damaging to the epithelium. The results of irritation studies indicated that lomefloxacin HCl nanosuspensions and drug-free CS nanosuspensions had no signs of redness, swelling, or increased production of tear fluid during treatment period. Transverse sections (T.S.) of rabbit's conjunctiva showed normal epithelium with intact goblet cells, no inflammatory reactions were observed (Fig. 6a–c). Histopathological examination of rabbit's corneas showed that no abnormal changes in corneas were observed after installation of the nanosuspensions (Fig. 6d–f). The corneal tissues had normal thickness and the blood vessels of ciliary body were of normal appearance. The above results indicated that the materials used in formulation of LF nanosuspensions were biocompatible with ocular tissues and hence can be safely used in ocular delivery.

Microbiological Activity

The results of the antibacterial activity of the optimized nanosuspension formulation were shown in Fig. 7. The measured MIC for LF solution was 11.7 μg/mL in case of *B. subtilis* and 0.7 μg/mL in case of *E. coli*, indicating that

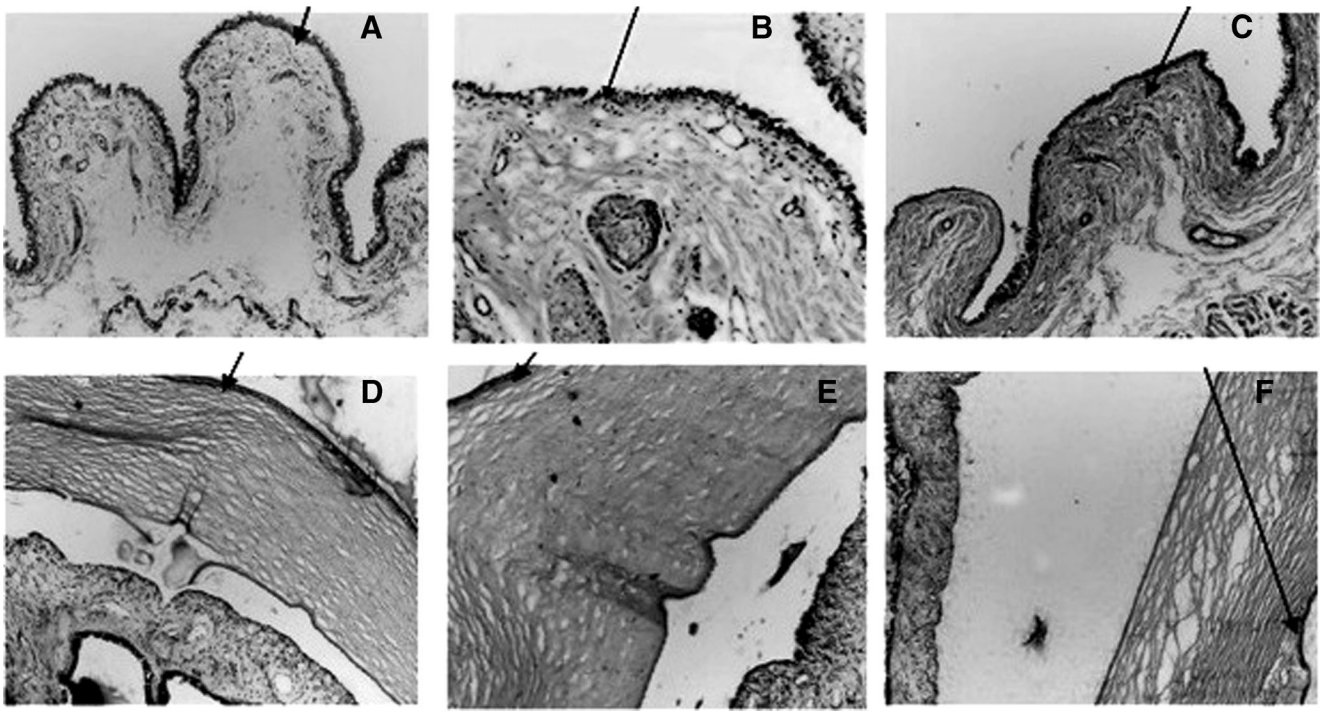

Fig. 6 Transverse sections in conjunctiva (**a** control, **b** LF solution group, and **c** LF nanosuspension group) and cornea of rabbit eye (**d** control, **e** LF solution group, and **f** LF nanosuspension group)

the drug is more effective against Gram-negative bacteria. However, the MIC of the optimized nanosuspension was 5.9 μg/mL in case of *Bacillus* and 0.2 μg/mL in case of *E. coli*. This large difference (about twofold decrease in MIC with *Bacillus subtilis* and threefold with *E. coli*) indicated the superior properties of the nanosuspension formulation. Also, the measured MBC of LF solution was 31.25 μg/mL in case of *B. subtilis* and 1.95 μg/mL in case of *E. coli*, However, the nanosuspension showed lower MBC of 15.6 and 0.97 μg/mL against *B. subtilis* and *E. coli*, respectively, confirming the above results of MIC. The higher antibacterial effect of LF nanosuspension compared to drug solution could be attributed to two reasons: firstly, the antimicrobial activity of chitosan by itself might have augmented the effects of LF [51]. Secondly, the increased permeability of the nanoparticles to the bacterial cell membrane enhanced by chitosan could have increased the antimicrobial activity of the whole formula. Although the antimicrobial effects of chitosan are not fully explained in the literature, some researchers suggested that the possible interaction between the positively charged chitosan molecules and the negatively charged bacterial cell wall can lead to its rupture [52]. Another suggestion relates chitosan antibacterial properties to its ability to chelate metal ions and this action can lead to intoxication of bacterial cells [53]. This later property is also exhibited by lomefloxacin where it forms chelates with heavy metals such as copper and magnesium leading to enhanced photostability and antimicrobial activity, respectively [54, 55]. In the nanosuspension formulation reported here, chitosan and lomefloxacin might have undergone chelation or complexation with each other through electrostatic interaction leading to improved activity as previously reported for chitosan and ofloxacin [56]. The prolonged duration and high permeability of nanoparticles resulted in higher antibacterial activity of the optimized nanosuspension compared to the drug solution.

Conclusion

The possibility of augmented antimicrobial activity of lomefloxacin HCl with chitosan was achieved not only through crosslinking and added antibacterial effects of chitosan but also through optimized nanosized particles. Lomefloxacin HCl nanosuspension with good entrapment efficiency, small particle size, and zeta potential was obtained through modeling and optimization of the formulation parameters. The optimized nanosuspension can prolong drug release, increase drug permeation, increase adherence to eye tissues, and hence maximize the ocular antimicrobial effects of the drug. Chitosan played the major role in the enhancement of both antimicrobial and transcorneal permeation of LF. The enhanced antibacterial action of LF nanosuspension revealed that such delivery system can be a good choice for highly effective treatment against ocular bacterial infections.

Acknowledgments A special acknowledgment is directed to the engineer, Mr. Stephen Roskily, previously working for Intelligensys Ltd., UK, for his help in using of the software (INForm). The authors also want to acknowledge the help given by Dr. Ahmed Osama El-Gendi at Beni-Suef University for help given during the microbiological study.

Ethical Standards All experiments done in this research on animals were performed according to the laws adopted by the ethical research committee of Beni-Suef University, Egypt.

Conflict of Interest The authors of this work declare that they have no conflict of interest.

References

1. Sultana N, Arayne MS, Furqan H. In vitro availability of lomefloxacin hydrochloride in presence of essential and trace elements. Pak J Pharm Sci. 2005;18:59–65.
2. Volpe DA. Permeability classification of representative fluoroquinolones by a cell culture method. AAPS Pharm Sci. 2004;6:1–6.
3. Klosinska-Szmurlo E, Grudzien M, Betlejewska-Kielak K, Plucinski FA, Biernacka J, Mazurek AP. Physico-chemical properties of lomefloxacin, levofloxacin and moxifloxacin relevant to Biopharmaceutics Classification System. Acta Chim Slov. 2014;61:827–34.
4. Sun J, Sakai S, Tauchi Y, Deguchi Y, Chen J, Zhang R, et al. Determination of lipophilicity of two quinolone antibacterials, ciprofloxacin and grepafloxacin, in the protonation equilibrium. Eur J Pharm Biopharm. 2002;54:51–8.
5. Volgyi G, Vizseralek G, Takacs-Novak K, Avdeef A, Tam KY. Predicting the exposure and antibacterial activity of fluoroquinolones based on physicochemical properties. Eur J Pharm Sci. 2012;47:21–7.
6. Mishra GP, Bagui M, Tamboli V, Mitra AK. Recent applications of liposomes in ophthalmic drug delivery. J Drug Deliv. 2011;2011:1–14.
7. Bucolo C, Maltese A, Drago F, eds. When nanotechnology meets the ocular surface. 2008;325–32.
8. Raju HB, Goldberg JL, eds. Nanotechnology for ocular therapeutics and tissue repair. 2008;431–6.
9. Badawi AA, El-Laithy HM, El Qidra RK, El Mofty H. Chitosan based nanocarriers for indomethacin ocular delivery. Arch Pharm Res. 2008;31:1040–9.
10. de la Fuente M, Ravia M, Paolicelli P, Sanchez A, Seijo BA, Alonso MJ. Chitosan-based nanostructures: a delivery platform for ocular therapeutics. Adv Drug Deliv Rev. 2010;62:100–17.
11. Kayser O, Lemke A, Hernandez-Trejo N. The impact of nanobiotechnology on the development of new drug delivery systems. Curr Pharm Biotechnol. 2005;6:3–5.
12. Mainardes RM, Urban MC, Cinto PO, Khalil NM, Chaud MV, Evangelista RC, et al. Colloidal carriers for ophthalmic drug delivery. Curr Drug Targets. 2005;6:363–71.
13. Ali M, Byrne ME. Challenges and solutions in topical ocular drug-delivery systems. Periodical. Challenges and solutions in topical ocular drug-delivery systems. 2008;1:145–61.
14. Pignatello R, Puglisi G. Nanotechnology in ophthalmic drug delivery: a survey of recent developments and patenting activity. Recent Pat Nanomedicine. 2011;1:42–54.

15. Del Amo EM, Urtti A. Current and future ophthalmic drug delivery systems: a shift to the posterior segment. Drug Discov Today. 2008;13:135–43.
16. Durairaj C, Kadam RS, Chandler JW, Hutcherson SL, Kompella UB. Nanosized dendritic polyguanidilyated translocators for enhanced solubility, permeability, and delivery of gatifloxacin. Invest Ophthalmol Vis Sci. 2010;51:5804–16.
17. Alonso MJ, Sanchez A. The potential of chitosan in ocular drug delivery. J Pharm Pharmacol. 2003;55:1451–63.
18. Van der Merwe S, Verhoef J, Verheijden J, Kotze A, Junginger H. Trimethylated chitosan as polymeric absorption enhancer for improved peroral delivery of peptide drugs. Eur J Pharm Biopharm. 2004;58:225–35.
19. Di Colo G, Zambito Y, Burgalassi S, Nardini I, Saettone M. Effect of chitosan and of N-carboxymethylchitosan on intraocular penetration of topically applied ofloxacin. Int J Pharm. 2004;273:37–44.
20. Ahuja M, Verma P, Bhatia M. Preparation and evaluation of chitosan-itraconazole co-precipitated nanosuspension for ocular delivery. J Exp Nanosci. 2012;222:1–13.
21. Qi L, Xu Z, Jiang X, Hu C, Zou X. Preparation and antibacterial activity of chitosan nanoparticles. Carbohydr Res. 2004;339:2693–700.
22. Ali HS, Blagden N, York P, Amani A, Brook T. Artificial neural networks modelling the prednisolone nanoprecipitation in microfluidic reactors. Eur J Pharm Sci. 2009;37:514–22.
23. Esmaeilzadeh-Gharedaghi E, Faramarzi MA, Amini MA, Rouholamini Najafabadi A, Rezayat SM, Amani A. Effects of processing parameters on particle size of ultrasound prepared chitosan nanoparticles: an artificial neural networks study. Pharm Dev Technol. 2012;17:638–47.
24. Amini MA, Faramarzi MA, Mohammadyani D, Esmaeilzadeh-Gharehdaghi E, Amani A. Modeling the parameters involved in preparation of PLA nanoparticles carrying hydrophobic drug molecules using artificial neural networks. J Pharm Innov. 2013;8:111–20.
25. Motwani SK, Chopra S, Talegaonkar S, Kohli K, Ahmad FJ, Khar RK. Chitosan-sodium alginate nanoparticles as submicroscopic reservoirs for ocular delivery: formulation, optimisation and in vitro characterisation. Eur J Pharm Biopharm. 2008;68:513–25.
26. Misra R, Acharya S, Dilnawaz F, Sahoo SK. Sustained antibacterial activity of doxycycline-loaded poly (D, L-lactide-co-glycolide) and poly (ε-caprolactone) nanoparticles. Nanomedicine. 2009;4:519–30.
27. Wu Y, Yang W, Wang C, Hu J, Fu S. Chitosan nanoparticles as a novel delivery system for ammonium glycyrrhizinate. Int J Pharm. 2005;295:235–45.
28. Liu H, Gao C. Preparation and properties of ionically cross-linked chitosan nanoparticles. Polym Adv Technol. 2009;20:613–9.
29. Abdelkader H, Ismail S, Kamal A, Alany RG. Design and evaluation of controlled release niosomes and discomes for naltrexone hydrochloride ocular delivery. J Pharm Sci. 2011;100:1833–46.
30. Gupta AK, Madan S, Majumdar D, Maitra A. Ketorolac entrapped in polymeric micelles: preparation, characterisation and ocular anti-inflammatory studies. Int J Pharm. 2000;209:1–14.
31. Mitragotri S, Anissimov YG, Bunge AL, Frasch HF, Guy RH, Hadgraft J, Kasting GB, Lane ME, Roberts MS. Mathematical models of skin permeability: an overview. Int J Pharm. 418: 115–29.
32. Gupta H, Aqil M, Khar R, Ali A, Bhatnagar A, Mittal G. Biodegradable levofloxacin nanoparticles for sustained ocular drug delivery. J Drug Target. 2011;19:409–17.
33. Luo Q, Zhao J, Zhang X, Pan W. Nanostructured lipid carrier (NLC) coated with chitosan oligosaccharides and its potential use in ocular drug delivery system. Int J Pharm. 2011;403:185–91.
34. Viertler C, Groelz D, Gündisch S, Kashofer K, Reischauer B, Riegman PHJ, et al. A new technology for stabilization of biomolecules in tissues for combined histological and molecular analyses. J Mol Diagn. 2012;14:458–66.
35. Colbourn E, Roskilly S, Rowe R, York P. Modelling formulations using gene expression programming—a comparative analysis with artificial neural networks. Eur J Pharm Sci. 2011;44:366–74.
36. Shao Q, Rowe RC, York P. Comparison of neurofuzzy logic and neural networks in modelling experimental data of an immediate release tablet formulation. Eur J Pharm Sci. 2006;28:394–404.
37. Ali AMA, Abdelrahim MEA. Modeling and optimization of terbutaline emitted from a dry powder inhaler and influence on systemic bioavailability using data mining technology. J Pharm Innov. 2014;9:38–47.
38. Kahlmeter G, Brown DF, Goldstein FW, MacGowan AP, Mouton JW, sterlund A, et al. European harmonization of MIC breakpoints for antimicrobial susceptibility testing of bacteria. J Antimicrob Chemother. 2003;52:145–8.
39. Ahmed SH, Amin MA, Saafan AE, El-Gendy AO, ul Islam M. Measuring susceptibility of Candida albicans biofilms towards antifungal agents. Der Pharm Lett. 2013;5:376–83.
40. Rajan M, Raj V. Encapsulation, characterisation and in-vitro release of anti-tuberculosis drug using chitosan-poly ethylene glycol nanoparticles. Int J Pharm Sci. 2012;4:255–9.
41. Gan Q, Wang T. Chitosan nanoparticle as protein delivery carrier: systematic examination of fabrication conditions for efficient loading and release. Colloids Surf B. 2007;59:24–34.
42. Boonsongrit Y, Mitrevej A, Mueller BW. Chitosan drug binding by ionic interaction. Eur J Pharm Biopharm. 2006;62:267–74.
43. Kumar D, Jain N, Gulati N, Nagaich U. Nanoparticles laden in situ gelling system for ocular drug targeting. J Adv Pharm Technol Res. 2013;4:9.
44. Agnihotri SA, Mallikarjuna NN, Aminabhavi TM. Recent advances on chitosan-based micro-and nanoparticles in drug delivery. J Control Release. 2004;100:5–28.
45. Zhang J, Chen XG, Li YY, Liu CS. Self-assembled nanoparticles based on hydrophobically modified chitosan as carriers for doxorubicin. Nanomed Nanotechnol. 2007;3:258–65.
46. Xu Y, Du Y. Effect of molecular structure of chitosan on protein delivery properties of chitosan nanoparticles. Int J Pharm. 2003;250:215–26.
47. Katas H, Alpar HO. Development and characterisation of chitosan nanoparticles for siRNA delivery. J Control Release. 2006;115:216–25.
48. Soppimath KS, Aminabhavi TM, Kulkarni AR, Rudzinski WE. Biodegradable polymeric nanoparticles as drug delivery devices. J Control Release. 2001;70:1–20.
49. Majumdar S, Hippalgaonkar K, Repka MA. Effect of chitosan, benzalkonium chloride and ethylenediaminetetraacetic acid on permeation of acyclovir across isolated rabbit cornea. Int J Pharm. 2008;348:175–8.
50. De Campos AM, Sanchez A, Alonso MJ. Chitosan nanoparticles: a new vehicle for the improvement of the delivery of drugs to the ocular surface. Application to cyclosporin A. Int J Pharm. 2001;224:159–68.
51. Vega E, Gamisans F, Garcia M, Chauvet A, Lacoulonche F, Egea M. PLGA nanospheres for the ocular delivery of flurbiprofen: drug release and interactions. J Pharm Sci. 2008;97:5306–17.
52. Benhabiles M, Salah R, Lounici H, Drouiche N, Goosen M, Mameri N. Antibacterial activity of chitin, chitosan and its oligomers prepared from shrimp shell waste. Food Hydrocoll. 2012;29:48–56.
53. Martinez LR, Mihu MR, Han G, Frases S, Cordero RJ, Casadevall A, et al. The use of chitosan to damage Cryptococcus neoformans biofilms. Biomaterials. 2010;31:669–79.
54. Fernandes P, Sousa I, Cunha-Silva L, Ferreira M, de Castro B, Feio MJ, et al. Synthesis, characterization and antibacterial studies of a copper (II) levofloxacin ternary complex. J Inorg Biochem. 2014;110:64–71.

55. Sadeek SA, El-Shwiniy WH, El-Attar MS, Zordok WA. Spectroscopic, structural and antibacterial evaluation of some lomefloxacin metal complexes. Int J Adv Res. 2014;2:158–208.

56. Singh J, Dutta PK. Preparation, antibacterial and physicochemical behavior of chitosan/ofloxacin complexes. Int J Polym Mater Polym Biomater. 2010;59:793–807.